Tunable superlensing by a mechanically controlled photonic crystal

Qi Wu, Ethan Schonbrun, and Wounjhang Park

Department of Electrical and Computer Engineering, University of Colorado, Boulder, Colorado 80309-0425

Received July 18, 2005; revised September 13, 2005; accepted September 22, 2005

We investigated negative refraction and subwavelength imaging by a mechanically tunable photonic crystal (PC) slab. A honeycomb-structured PC composed of a silicon–polyimide membrane was used because it exhibits isotropic negative refraction within the second photonic band. Using the finite-difference time-domain (FDTD) method, we demonstrated focusing properties of the PC lenses at various frequencies and mechanical stresses. Analyses based on a ray optics model and equifrequency surface also confirmed the behavior observed by the FDTD simulations. These results suggested a mechanically tunable superlens, whose achievable frequency bandwidth was 12.9% of the center frequency for a mechanical stress of ±10%. © 2006 Optical Society of America

OCIS codes: 350.3950, 160.4670, 260.2110.

Negative refraction refers to an unconventional optical phenomenon in which electromagnetic waves are bent in directions opposite to what are normally observed in regular dielectric materials. This novel phenomenon was first perceived by Veselago[1] and rediscovered recently by Pendry.[2] A negative-index material creates a lens with flat surfaces and, more importantly, subwavelength imaging, which refers to the capability of reconstructing an image with resolutions smaller than the light wavelength. This is possible because the evanescent waves are amplified in the negative-index material and thus contribute to the reconstruction of the image. The capability of overcoming the diffraction limit on resolution presents exciting possibilities for numerous novel applications, and therefore negative refraction has been the subject of extensive research.

There are two types of material in which negative refraction is predicted or observed-metamaterials and photonic crystals (PCs). Metamaterials refer to artificially constructed materials composed of arrays of features with dimensions much smaller than the light wavelength. For negative refraction, metamaterials consisting of conducting wires and split-ring resonators have been investigated.[3] Metamaterials can possess simultaneously negative ϵ and μ and therefore exhibit left-handed behavior. Negative refraction and focusing by negative-index metamaterials have been experimentally demonstrated in the microwave frequency region.[3,4] Recently, the transmission, reflection, and absorption properties of slabs of split-ring-type resonators were investigated numerically at infrared and optical frequencies, showing that the resonator possesses a negative refractive index near the resonant frequency of the rings.[5] Nanostructured magnetic resonators exhibiting resonances in the mid-infrared spectral region were experimentally demonstrated, and the possibility of extending the negative permeability to optical frequencies was discussed. Although these recent developments are exciting and remarkable, the elaborate construction of a medium containing a periodic array of wires and ring resonators makes their fabrication a complicated process, and thus extension of their operating frequency into the optical regime still remains a formidable task.

In view of the relative ease of fabrication, the possibility of optical frequency operation, and low loss, PCs provide an excellent alternative. PCs may exhibit negative refraction through two distinct mechanisms. The first case is when the PC possesses a positive effective index but exhibits negative refraction owing to the negative curvature of the dispersion surface.[7] The second possibility is that the PC actually possesses a negative effective index and thus behaves like a left-handed material.[8] Subwavelength imaging was theoretically demonstrated in both cases.

A critical improvement needed for practical application of a negative-index material is to achieve tunability. Negative refraction is a resonant phenomenon and therefore exhibits acute frequency dependence. This places a severe limitation on the operating frequency range, and it is obvious that achieving broadband operation would greatly expand the utility of negative-index materials. Several schemes have been proposed to tune the properties of the PCs by modifying their refractive index contrast. They include infiltrating with liquid crystals,[9,10] changing temperature,[11] using the Kerr effect,[12] and incorporating electro-optic materials such as ferroelectric lead lanthanum zirconate titanate.[13] Although successfully demonstrated, these schemes tend to provide relatively small tunability owing to the small achievable change in refractive index. To achieve greater tunability, we investigated a new scheme, in our opinion, by employing the mechanically tunable PC concept recently proposed by Park and Lee.[14] Taking advantage of the fact that the photonic band structure is extremely sensitive to the lattice structure, this scheme uses mechanical stress to modify the PC lattice and thus control the optical properties of PCs. We have theoretically demonstrated the wide tunability attainable with this new PC structure for

0740-3224/06/030479-6/$15.00

both beam steering[14] and negative-index imaging.[15] We have also experimentally observed negative refraction at 1.54 μm in a mechanically tunable Si–polyimide PC membrane.[16]

In our previous study of mechanical tuning of negative-index imaging, we used the PC structure with a positive effective index but showing negative curvature in the dispersion curve.[15] In this paper, we investigate the effect of mechanical stress on a PC structure possessing a circular dispersion surface and thus exhibiting isotropic negative refraction. Wang *et al.* recently reported that superlensing is unrestricted in this type of PC.[17] We began our search for a PC structure exhibiting isotropic negative refraction by examining the triangular array of Si pillars ($n=3.46$) in a flexible polymer film such as polyimide ($n=1.5$). In this structure, the second band for TM polarization shows a circular equifrequency surface (EFS) that shrinks with increasing frequency, thereby exhibiting isotropic negative refraction. However, we found that there also exists an anisotropic third band that overlaps the second band and, consequently, compromises the isotropic negative refraction due to the second band, as shown by Fig. 1(a). We note that this is in contrast to the triangular lattice of air holes in a high-index material, which has been studied by many groups before. In the air-hole structure, the second and third bands are well separated, and thus the isotropic negative refraction due to the second band is not complicated by other bands. This preferred band structure of the air-hole PC structure, however, is not applicable in our case. To be able to mechanically tune the PC lattice, we must have a flexible polymer film as a background dielectric material, which forbids us from using an air-hole PC structure and limits us to using a dielectric rod PC structure.

A close examination of the band structure of the triangular lattice of Si rods embedded in polyimide shows that the second and third bands are degenerate at the high symmetry points of Γ and K. Figure 1(b) shows the two normal mode-field patterns for the degenerate second band at the Γ point. Both modes have an antinode in the middle of the Si rod, but in one case the antinode is oriented along the $\Gamma-M$ direction and in the other along the $\Gamma-K$ direction. To lift the degeneracy and therefore to separate the third band from the second band, it is necessary to lower the symmetry so that the two field patterns possess different energies. One way to achieve this symmetry lowering is to use a honeycomb lattice, which is a triangular lattice with two Si rods per unit cell. When we construct a honeycomb lattice by placing two Si rods along the $\Gamma-K$ direction, the two field patterns in Fig. 1(b) should represent two different energy states. As shown in Fig. 1(c), the fields are concentrated in the high-index region in one case (bottom panel), whereas antinodes are formed across the two Si rods in the other case (top panel). Now it can be seen easily that the former case should have much lower energy than the latter. Indeed, our photonic band-structure calculation revealed that the former case corresponds to the second band of the honeycomb lattice, and the latter is the sixth band.

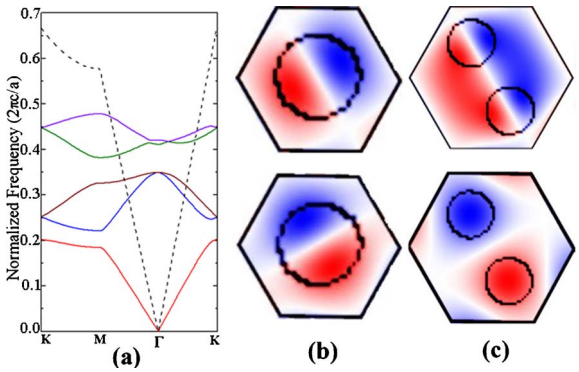

Fig. 1. (Color online) (a) Photonic band structure (TM mode) for a two-dimensional (2D) PC with a hexangular structure. The black dashed curve in (a) is the light dispersion curve in air. (b) E_z field patterns for the second band of a triangular lattice of Si rods in polyimide and (c) the second (bottom) and sixth (top) bands of a honeycomb lattice. The hexagonal boundary defines the Wigner–Seitz unit cell.

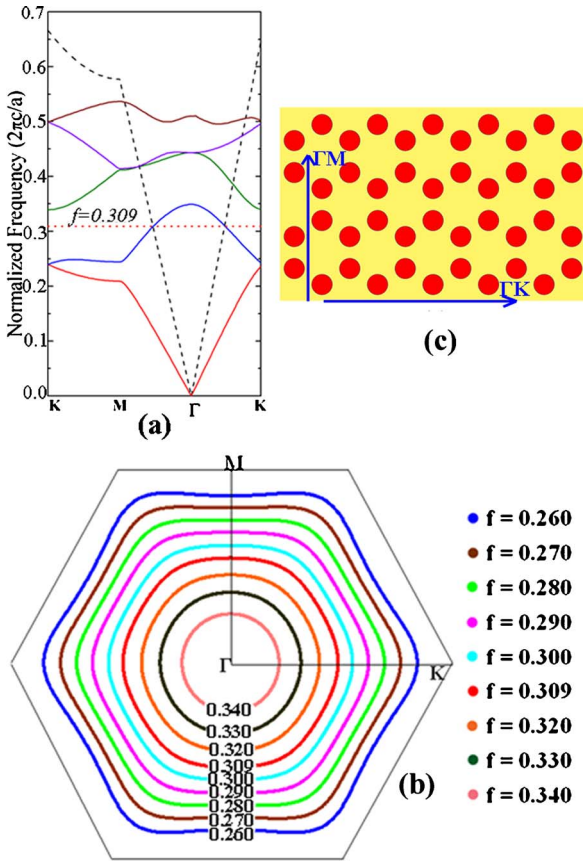

Fig. 2. (Color online) (a) Photonic band structure and (b) EFSs for a 2D PC with a honeycomb structure. Both of them are for TM modes. The black dashed curve in (a) is the light dispersion curve in air. The horizontal red dotted line represents a frequency of 0.309 where the light dispersion curve in air intersects with the second photonic band. (c) The schematic of the honeycomb structure composed of Si rods (with diameter as $0.8a$) in polyimide. The lattice orientation $\Gamma-K$ and $\Gamma-M$ are also shown.

The two-dimensional (2D) honeycomb lattice of Si rods in polyimide we investigated in this study is schematically shown in Fig. 2(c). The radius of silicon rods was set to be $r=0.4a$, where a is the distance between two nearest-neighbor rods. Note that the actual lattice constant is $a_0=\sqrt{3}a$ and we used $2\pi c/a_0$ as the frequency unit throughout this paper. We employed the plane-wave ex-

pansion method to calculate the photonic band structure and the EFSs.[18] The band structure in Fig. 2(a) clearly shows that the second band is well separated from the third band, as anticipated from the preceding discussion. Also, the EFSs were found to be circular near the bandgap and gradually changed to a hexagonal shape as the frequency was decreased, as shown in Fig. 2(b). The EFSs became smaller with increasing frequency, which is the characteristic behavior of a negative refraction regime. We therefore expect uninterfered negative refraction due to the second band in a wide range of frequency. The band structure we presented here corresponds to a 2D PC with infinitely long rods. We recognize that we have to consider a 2D PC slab with a finite thickness for practical device applications. The band structure of a 2D PC slab with a finite thickness can be adequately described by a 2D PC with an effective index. In this case, one should take into account the strong frequency dependence of the effective index, which may cause the actual band structure to severely deviate from the pure 2D modeling. However, this will not cause serious problems in our case, thanks to the design flexibility of PCs. The frequency range in which the PC exhibits negative refraction is relatively narrow. Therefore, one can design a negative-index PC structure targeted to a particular frequency range and use the effective index for that frequency range in the 2D modeling. This way, 2D modeling can still be used to adequately describe the negative refraction in a 2D PC slab with a finite thickness. In this paper, we investigated the frequency range of 0.29–0.33 (in the unit of $2\pi c/a_0$). Also, we used the materials' dielectric constants in our theoretical modeling, since we can easily change them to effective indices given the geometry size of the PC slab and the desired operating frequencies.

That the EFSs are circular near the top of the second band indicates that the refraction in the PC is isotropic, and we can therefore define a meaningful effective index.[19] By taking the PC slab as an isotropic material with a negative refractive index, we can trace the ray propagation through the PC and predict the image position for a given source position. Assuming the incident light ray has an incident angle of θ_{inc} and the corresponding refractive angle inside the PC is θ_{PC}, we obtain an equation that describes the lens: $(d_1+d_2)\tan\theta_{\text{inc}} = t\tan\theta_{\text{PC}}$. Here d_1 and d_2 are the distances between the source and the PC and between the PC and the image, respectively, and t is the thickness of the PC slab. From Snell's law, we then find

$$(d_1 + d_2) + (t/n_{\text{eff}})(\cos\theta_{\text{inc}}/\cos\theta_{\text{PC}}) = 0. \quad (1)$$

The cosine term represents the contribution from the rays with large incident angles, causing the focus to spread along the optic axis. It may be ignored for paraxial rays. When $n_{\text{eff}}=-1$, the term $(\cos\theta_{\text{inc}}/\cos\theta_{\text{PC}})$ becomes 1, and we can find a single solution for the image position (d_2) even for nonparaxial rays. The image quality along the propagation direction will thus be best when $n_{\text{eff}}=-1$. For other values of n_{eff}, the ray model does not give a single, well-defined solution, but it does allow us to predict the trend. For $|n_{\text{eff}}|<1$, the second term in Eq. (1) will become larger, putting the image farther away from the negative-index PC lens. On the other hand, when the magnitude of n_{eff} is increased, the image would move toward the PC.

The black dashed curve in Fig. 2(a) is the light dispersion curve in air. It intersects the second band at $f=0.309$. The EFS curve at this frequency is shown in Fig. 2(b) by the red curve and was found to be nearly circular. This indicates that the PC structure will act like a homogeneous material with an effective index of -1 at this frequency. We can then predict the focusing property of the lens by Eq. (1). If we assume that our PC lens has a thickness of $3.2a_0$ and a point source is placed at a distance of $1.0a_0$ away from the PC, the image should be found at $2.2a_0$ from the PC lens. Note that the physical width of the PC slab along the $\Gamma-M$ direction may be modified owing to the lateral Goos–Hänchen-like shift.[20] For this, we estimated the effective width of our PC slab by performing finite-difference time-domain[21] (FDTD) simulations similar to those presented in Ref. 22. In these simulations, we measured the lateral shift of a Gaussian beam at various incident angles after it was transmitted through the PC slab and used the effective index obtained from the EFSs presented in Fig. 2(b) to calculate the effective width. The effective width was found to be close to the physical thickness of the PC slab, with deviations less than 5%. Therefore, we use the physical width of the PC slab in the remainder of this paper.

Given the frequency dependence of the EFS shown in Fig. 2(b) and on the basis of our ray-tracing analysis above, we expect the image should form farther away from the PC lens at a higher frequency. As the frequency is decreased, the magnitude of the effective index further increases, producing images closer to the PC. We also noted that the EFSs of a PC at higher frequencies are smaller than that in air, indicating that the PC lens will not be able to collect all the propagating components of the incident light regardless of its aperture size. This is going to affect the resolution of the image. Moreover, the modes within this frequency range are leaky in a 2D PC slab with a finite thickness, and they will not contribute to the formation of images. Consequently, despite the more isotropic negative refraction expected in this region, this is not an ideal regime to operate the negative-index PC lens. On the other hand, although the EFSs become slightly anisotropic at lower frequencies, a well-defined image with subwavelength resolution could still be obtained, as shown by the FDTD simulations later. In general, we want the intersection points between the light line and the photonic bands of the PC to be close to the top of the second band, so that we have a wide frequency range below where modes are confined in a 2D PC slab with a finite thickness and negative refraction is isotropic. This, in principle, can be achieved by one's properly choosing the lattice parameters and by the effective index, which is determined by the thickness of the 2D PC slab.

To directly visualize the focusing properties of the PC lens, we performed point-source imaging simulations using the FDTD method. The computational cell contained a PC slab of 17×2 primitive unit cells of the honeycomb lattice sandwiched between air regions. The PC was oriented in such a way that the air–PC interface is along the $\Gamma-K$

direction and the normal incidence corresponds to the $\Gamma-M$ direction. The computational domain was terminated with the perfectly matched layer boundary condition in order to avoid unphysical reflections from the computational cell boundaries.[23] We placed a continuous-wave point source at a distance $1.0a_0$ from the surface of the PC slab and varied the frequency from $\omega=0.295$ to 0.300, 0.305, 0.309, 0.315, and 0.320; as shown in Fig. 3, point images were found on the other side of the slab at distances of $0.8a_0$, $1.3a_0$, $1.8a_0$, $2.3a_0$, $3.3a_0$, and $4.0a_0$, respectively. The result for a frequency of 0.309 ($n_{\text{eff}}=-1$ case) agreed well with the ray optics model, and the image positions showed the correct frequency dependence as predicted by the analysis based on the EFSs and effective index. We also measured the transverse size (full width at half-maximum from a time-averaged intensity plot) of the images, and they were 0.47λ, 0.48λ, 0.48λ, 0.50λ, 0.55λ and 0.59λ, where λ is the source wavelength. The images all exhibited sizes below the source wavelength, demonstrating the subwavelength resolution achievable in this frequency range. We also note that the image size was larger for images formed farther away from the PC lens. This is because the evanescent component decays quickly after exiting the PC lens, thereby contributing less to the image formation.

The negative-index PC lens exhibits severe chromatic aberration, since the EFS is sensitive to the operating frequency. To tune the negative-index PC lens, we use mechanical stress, which modifies the EFS and, consequently, the focusing characteristics. In the following simulations, we assume mechanical stress is applied along the $\Gamma-K$ direction (perpendicular to the optic axis of the PC lens) and the dimension along the $\Gamma-M$ direction; i.e., the thickness of the PC lens is kept unchanged. We modeled three cases of stretching and compression by 2%, 5%, and 10%. Here, the 2% stretched lattice means that the distance between the two neighboring Si pillars is 2% longer than that in the unstressed honeycomb lattice.

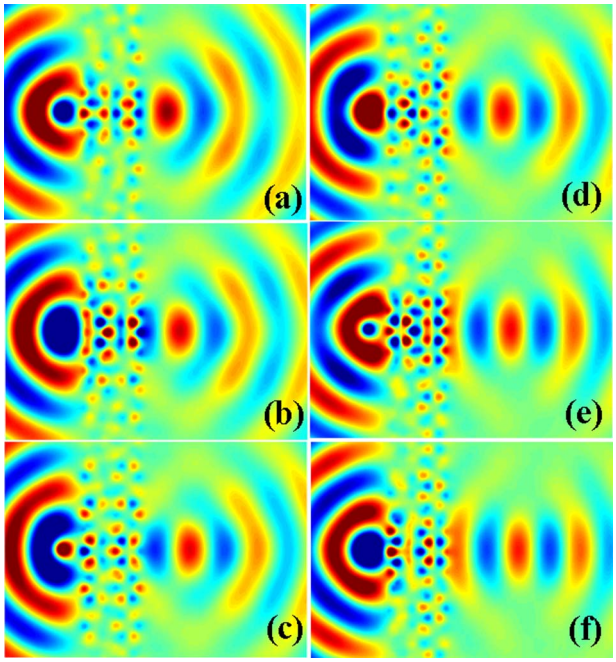

Fig. 3. (Color online) Electric field distribution of point sources and their images across a 2D honeycomb PC slab, at source frequencies of (a) 0.295, (b) 0.300, (c) 0.305, (d) 0.309, (e) 0.315, and (f) 0.320. Red and blue colors are used to represent the positive and negative fields. The locations of the point sources are at a distance of $1.0a_0$ from the left edge of the slab. Images move away from the PC lenses as the frequency is increased.

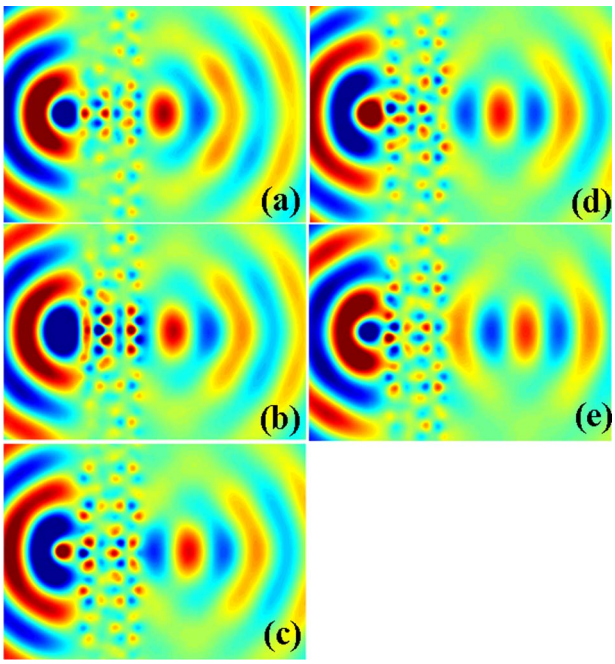

Fig. 4. (Color online) Electric field distribution of point sources and their images across a 2D honeycomb PC slab for various PC structures at a frequency of 0.305. The PCs are the (a) 5% compressed lattice, (b) 2% compressed lattice, (c) regular honeycomb lattice, (d) 2% stretched lattice, and (e) 5% stretched lattice. The positions of the sources are also at a distance of $1.0a_0$ from the left edge of the slabs.

We investigated the effect of mechanical stress on the focusing characteristics by performing FDTD simulations. All the PC lenses had the same lateral dimension as that of the unstressed honeycomb structure shown in Fig. 2(c), and the point sources were placed at the same distance of $1.0a_0$ from the edge of the PC lenses. Therefore, the difference in image properties among these cases arises only from the difference in the PC structure along the direction of mechanical stress. Figure 4 shows the focusing properties of various PC structures at a fixed frequency of 0.305. The general trend was that the image moved farther away from the PC lens as the PC structure was stretched. On the other hand, as the PC lattice was compressed, the image appeared closer to the PC slabs. In the unstressed honeycomb structure [Fig. 4(c)], the image was at a distance of $1.8a_0$ from the right edge of the slab. In the 2% and 5% stretched cases [Figs. 4(d) and 4(e)], images were located at $2.5a_0$ and $3.4a_0$ from the slab, respectively. In the 5% and 2% compressed cases [Figs. 4(a) and 4(b)], the distances between the image and the PC slab were $0.7a_0$ and $1.3a_0$. These results clearly showed that we could engineer the focusing property of the PC slab with relatively simple modification of its lattice structure. Again, we note that subwavelength resolution was achieved in all cases. The lateral sizes of the images were 0.42λ, 0.46λ, 0.48λ, 0.51λ, and 0.55λ. The observed

change in image size could once again be correlated well with the image distance, indicating that it is due to the decay of the evanescent waves.

We further investigated the focusing properties of the mechanically tuned PC lenses by examining their EFSs. Figure 5 shows the EFSs for various PC structures including 2% and 5% stretched and compressed lattices. We found the stretched lattices had smaller EFS curves than the unstressed honeycomb PC had. Conversely, the EFSs of compressed lattices were larger. Similarly to our previous discussion on the frequency dependence, smaller EFSs indicate a smaller effective index. Consequently, the image would be farther away from the PC, which was exactly what we found from the FDTD simulations. On the other hand, compressed lattices whose effective indices were larger would create images closer to the PC lens, again consistent with the FDTD simulations. Although the size of EFSs in Fig. 5 changed in response to applied mechanical stress, there was no noticeable change in the shape of the EFS curve. We can therefore conclude that in this case the mechanical stress changes only the effective index while preserving isotropic negative refraction.

Combining the frequency dependence and the mechanical stress effect, we can now design a tunable negative-index PC lens. Various FDTD simulation results are combined in Fig. 6 to demonstrate how the focusing properties of the PC slabs change with respect to frequency and mechanical stress. It can be seen clearly that, for each PC structure and the frequency range we studied, increasing the frequency makes the image move away from the slab; on the other hand, at a fixed frequency, compressing the PC pulls the image toward the slab, whereas stretching it pushes the image away from the PC. We make two observations from the data shown in Fig. 6. First, a vertical line means a fixed operating frequency. Its intersection points with the data curves define a range of an achievable focusing property by one's mechanically tuning the PC lens. This raises an interesting possibility of designing a tunable imaging system whose focal length can be tuned as needed. Second, a horizontal line in the figure represents a fixed image position, and the intersection points with our data curves determine the mechanical stress needed to obtain the desired image

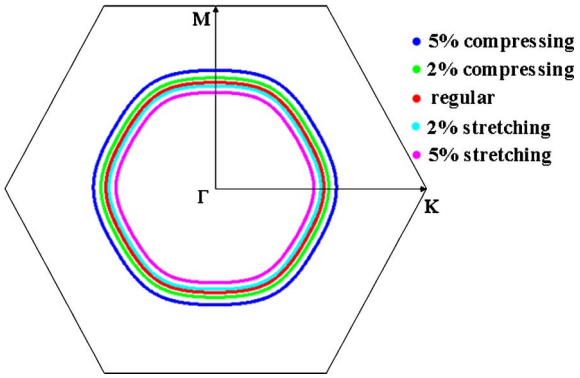

Fig. 5. (Color online) EFSs of various PC lattices at a frequency of 0.305. They are 5% (the outermost curve) and 2% (second from outside) compressed lattices, regular honeycomb lattice (middle curve), and 2% (second from inside) and 5% (the innermost curve) stretched lattices, which are the same structures we used to perform the FDTD simulation in Fig. 4.

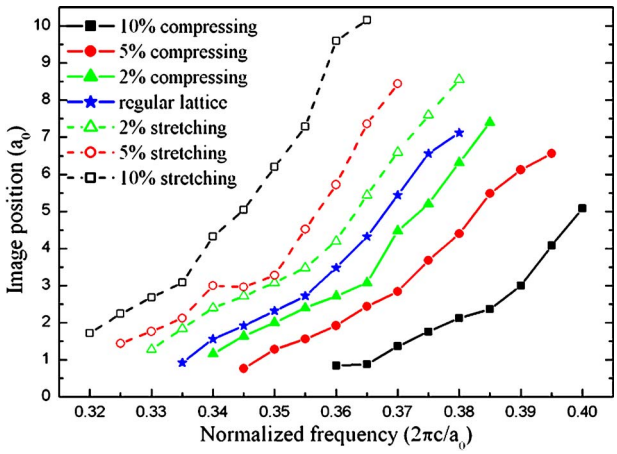

Fig. 6. (Color online) Focusing properties vary with PC slabs of different PC structures over a range of frequencies. Besides the regular honeycomb lattice, 2%, 5%, and 10% stretched and compressed lattices were examined as examples. PC structures are represented by curves with different colors and labels. The y axis is the distances between the imaging point and PC slab in the unit of lattice constant a_0.

distance at various frequencies. This data will allow us to design, for example, a frequency-scanning imaging system in which a mechanically tuned PC lens focuses various frequency components to a fixed detector. For example, for a fixed image distance of $2.3a_0$, we found the tunable frequency range was between 0.290 and 0.330 with mechanical stress up to ±10%. When we take the frequency of the unstressed honeycomb structure, 0.309, as the center, the mechanically tunable PC slab gives us an operating frequency bandwidth of 12.9% of the center frequency. This corresponds to a tunable bandwidth of 200 nm at the communication wavelength of 1.54 μm.

In conclusion, we investigated subwavelength imaging by mechanically tunable 2D honeycomb PC slabs. The honeycomb PC has an isolated second photonic band that exhibits isotropic negative refraction. The focusing property of the PC lens was found to be strongly dependent on frequency and the PC lattice structure. By combining the strong frequency dependence and high sensitivity to mechanical stress, we were able to construct a tunable negative-index lens. By using a relatively small mechanical stress of up to ±10%, we achieved a tunable bandwidth of 12.9% of the center frequency, which corresponds to 200 nm at the communication wavelengths.

Corresponding author W. Park can be reached by e-mail at won.park@colorado.edu.

REFERENCES

1. V. G. Veselago, "The electrodynamics of substances with simultaneously negative values of ϵ and μ," Sov. Phys. Usp. **10**, 509–514 (1968).
2. J. B. Pendry, "Negative refraction makes a perfect lens," Phys. Rev. Lett. **85**, 3966–3969 (2000).
3. R. A. Shelby, D. R. Smith, and S. Schultz, "Experimental verification of a negative index of refraction," Science **292**, 77–79 (2000).
4. A. A. Houck, J. B. Brock, and I. L. Chuang, "Experimental observations of a left-handed material that obeys Snell's law," Phys. Rev. Lett. **90**, 137401 (2003).
5. N. C. Panoiu and R. M. Osgood, "Influence of the dispersive

properties of metals on the transmission characteristics of left-handed materials," Phys. Rev. E **68**, 016611 (2003).
6. S. Zhang, W. Fan, B. K. Minhas, A. Frauenglass, K. J. Malloy, and S. R. J. Brueck, "Midinfrared resonant magnetic nanostructures exhibiting a negative permeability," Phys. Rev. Lett. **94**, 037402 (2005).
7. C. Luo, S. G. Johnson, J. D. Joannopoulos, and J. B. Pendry, "All-angle negative refraction without negative effective index," Phys. Rev. B **65**, 201104 (2002).
8. P. V. Parimi, W. T. Lu, P. Vodo, and S. Sridhar, "Imaging by flat lens using negative refraction," Nature **426**, 404 (2003).
9. K. Bush and S. John, "Liquid-crystal photonic-band-gap materials: the tunable electromagnetic vacuum," Phys. Rev. Lett. **83**, 967–970 (1999).
10. W. Park and C. J. Summers, "Optical properties of superlattice photonic crystal waveguides," Appl. Phys. Lett. **84**, 2013–2015 (2004).
11. K. Yoshino, Y. Shimoda, Y. Kawagishi, K. Nakayama, and M. Ozaki, "Temperature tuning of the stop band in transmission spectra of liquid-crystal infiltrated synthetic opal as tunable photonic crystal," Appl. Phys. Lett. **75**, 932–934 (1999).
12. N. C. Panoiu, M. Bahl, and R. M. Osgood, "Optically tunable superprism effect in nonlinear photonic crystals," Opt. Lett. **28**, 2503–2505 (2003).
13. D. Scrymgeour, N. Malkova, S. Kim, and V. Gopalan, "Electro-optic control of the superprism effect in photonic crystals," Appl. Phys. Lett. **82**, 3176–3178 (2003).
14. W. Park and J. B. Lee, "Mechanically tunable photonic crystal structure," Appl. Phys. Lett. **85**, 4845–4847 (2004).
15. Q. Wu and W. Park, "Broadband sub-wavelength imaging by mechanically tunable photonic crystal," J. Comput. Theor. Nanosci. **2**, 202–206 (2005).
16. E. Schonbrun, M. Tinker, W. Park, and J. B. Lee, "Negative refraction in a Si-polymer photonic crystal membrane," IEEE Photon. Technol. Lett. **17**, 1196–1198 (2005).
17. X. Wang, Z. F. Ren, and K. Kempa, "Unrestricted superlensing in a triangular two-dimensional photonic crystal," Opt. Express **12**, 2919–2924 (2004).
18. S. G. Johnson and J. D. Joannopoulos, "Block-iterative frequency-domain methods for Maxwell's equations in a planewave basis," Opt. Express **8**, 173–191 (2001).
19. M. Notomi, "Theory of light propagation in strongly modulated photonic crystals: refractionlike behavior in the vicinity of the photonic band gap," Phys. Rev. B **62**, 10696–10705 (2000).
20. D. Felbacq and R. Smaâli, "Block modes dressed by evanescent waves and the generalized Goos–Hänchen effect in photonic crystals," Phys. Rev. Lett. **92**, 193902 (2004).
21. K. S. Yee, "Numerical solution of initial boundary value problems involving Maxwell's equations in isotropic media," IEEE Trans. Antennas Propag. **14**, 302–307 (1966).
22. A. Martínez and J. Martí, "Negative refraction in two-dimensional photonic crystals: role of lattice orientation and interface termination," Phys. Rev. B **71**, 235115 (2005).
23. J. P. Berenger, "A perfectly matched layer for the absorption of electromagnetic waves," J. Comput. Phys. **114**, 185–200 (1994).